Photoinduced Carrier Generation and Recombination Dynamics of a Trilayer Cascade Heterojunction Composed of Poly(3-hexylthiophene), Titanyl Phthalocyanine, and C 60

ARTICLE *in* THE JOURNAL OF PHYSICAL CHEMISTRY B · APRIL 2015

Impact Factor: 3.3 · DOI: 10.1021/acs.jpcb.5b00110 · Source: PubMed

3 AUTHORS:

Jaehong Park

National Renewable Energy Laboratory

12 PUBLICATIONS **184** CITATIONS

SEE PROFILE

Obadiah G. Reid

University of Colorado Boulder

27 PUBLICATIONS **912** CITATIONS

SEE PROFILE

Garry Rumbles

National Renewable Energy Laboratory

208 PUBLICATIONS **6,414** CITATIONS

SEE PROFILE

THE JOURNAL OF PHYSICAL CHEMISTRY B

Article

pubs.acs.org/JPCB

Photoinduced Carrier Generation and Recombination Dynamics of a Trilayer Cascade Heterojunction Composed of Poly(3-hexylthiophene), Titanyl Phthalocyanine, and C_{60}

Jaehong Park,[†] Obadiah G. Reid,[†,‡] and Garry Rumbles*[,†,‡]

[†]Chemical and Materials Science Center, National Renewable Energy Laboratory, 15013 Denver West Parkway, Golden, Colorado 80401, United States

[‡]Department of Chemistry and Biochemistry, and Renewable and Sustainable Energy Institute, University of Colorado at Boulder, Boulder, Colorado 80309, United States

Supporting Information

ABSTRACT: We use flash-photolysis time-resolved microwave conductivity experiments (*FP*-TRMC) and femtosecond−nanosecond pump−probe transient absorption spectroscopy to investigate photoinduced carrier generation and recombination dynamics of a trilayer cascade heterojunction composed of poly(3-hexylthiophene) (P3HT), titanyl phthalocyanine (TiOPc), and fullerene (C_{60}). Carrier generation following selective photoexcitation of TiOPc is independently observed at both the P3HT/TiOPc and TiOPc/C_{60} interfaces. The transient absorption results indicate that following initial charge generation processes to produce $P3HT^{\bullet+}/TiOPc^{\bullet-}$ and $TiOPc^{\bullet+}/C_{60}^{\bullet-}$ at each interface from (P3HT/TiOPc*/C_{60}), the final charge-separated product of ($P3HT^{\bullet+}$/TiOPc/$C_{60}^{\bullet-}$) is responsible for the long-lived photoconductance signals in *FP*-TRMC. At the P3HT/TiOPc interface in both P3HT/TiOPc and P3HT/TiOPc/C_{60} samples, the electron transfer appears to occur only with the crystalline (weakly coupled H-aggregate) phase of the P3HT.

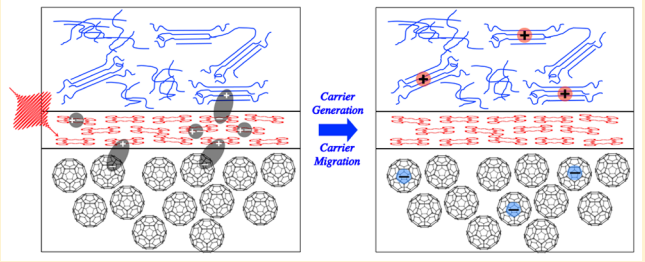

INTRODUCTION

Our fundamental understanding of photoinduced electron transfer in organic solids has progressed substantially in the last three decades.[1−18] Concurrently, certified efficiencies of organic photovoltaic (OPV) devices have increased from ∼1% in 1984 to 12% in 2014.[19] Nevertheless, new device architectures that go beyond binary mixtures and bilayers favored in the past will likely be needed to push the efficiency of OPV devices higher. Ternary (or higher order) blend solar cells are a promising alternative to binary composites because of the potential for better absorption of the solar spectrum and thus higher short circuit current.[20−32] In spite of this advantage, it is yet to be elucidated how additional components impact photoinduced carrier generation and recombination processes. For example, one might expect that planar ternary junctions would exhibit slower charge recombination kinetics than bilayers because the central layer acts as a barrier to recombination, which could allow enhanced open circuit voltage and/or fill-factor in devices. Such hypotheses have not been tested. Therefore, more fundamental work is clearly required to fully understand the operating mechanism of these ternary systems and their potential advantages over binary systems.

In this work we study the photoinduced carrier generation and recombination dynamics between constituents of a model ternary composite and the subsequent dynamics in ternary systems where a second charge-transfer step may occur. Our model system is a trilayer cascaded heterojunction composed of titanyl phthalocyanine (TiOPc) sandwiched between regioregular poly(3-hexylthiophene) (RR-P3HT) and C_{60}. Because of the simplicity of its morphology and well-defined interface, a trilayer system can be advantageous for interrogating photoinduced carrier generation and recombination dynamics over popular bulk heterojunction structures that may exhibit more complicated excited-state dynamics due to their complex, poorly understood microstructure. Because phthalocyanines (Pc) have high extinction coefficients (>10^5 $M^{-1}cm^{-1}$) in the near-infrared (NIR), Pc derivatives are attractive as a photon-capturing layer. Recently, Placencia et al. reported AM 1.5G efficiencies of ∼1.4% of the as-deposited TiOPc/C_{60} bilayer and ∼4% when the TiOPc is crystallized.[33] Thus, the trilayer structure P3HT/TiOPc/C_{60} serves as an interesting model, possessing both structural simplicity and efficient photoinduced carrier generation.

TiOPc has broad Q-band absorption in the NIR (Figure 1B) whereas the RR-P3HT and C_{60} exhibits absorption in the visible (Figure 1A,C), providing continuous strong absorption from 300 to 800 nm (Figure 2). In addition, the electron

Special Issue: John R. Miller and Marshall D. Newton Festschrift

Received: January 5, 2015
Revised: April 13, 2015
Published: April 20, 2015

DOI: 10.1021/acs.jpcb.5b00110
J. Phys. Chem. B 2015, 119, 7729−7739

affinity and ionization potentials of the TiOPc are situated between those of the P3HT and those of C_{60}: TiOPc* is an electron acceptor relative to P3HT and an electron donor relative to C_{60}; likewise, it is a hole donor relative to P3HT and a hole acceptor relative to C_{60}. These energy levels are shown approximately in Figure 1D.

To explore excited-state dynamics, we use flash-photolysis time-resolved microwave conductivity (*FP*-TRMC) and femtosecond and nanosecond pump−probe transient absorption spectroscopy (fsTA and nsTA, respectively).

FP-TRMC is useful for investigating charge carrier dynamics in the nanosecond-microsecond time domain;[8,9,34−36] it provides a contactless probe of photoconductivity sensitive enough for use at very low excitation fluence conditions (<10^{12} photon/cm^2). However, the time resolution is relatively poor (∼5 ns), and it can be difficult to separate yield and mobility contributions to the photoconductivity.

On the other hand, pump−probe transient absorption spectroscopy is an extremely versatile tool for probing exciton and carrier dynamics[5,28,37−40] because of the ability to spectrally separate distinct species and the femtosecond time resolution that is routinely achieved. Yet, in spite of its several advantages, the higher excitation fluence necessary for TA experiments leads inevitably to many-body interactions, including exciton−exciton and/or exciton−carrier interactions that make connecting the measured dynamics with conditions approaching solar flux quite difficult. Moreover, it can be difficult to assign the myriad spectral features that arise in the transient spectra. TRMC provides a bridge to lower fluence and the useful specificity of being sensitive only to mobile charges. Thus, combination of *FP*-TRMC and TA techniques can provide unique insight into exciton and carrier dynamics from femtosecond to microsecond time domain.[41]

Carrier generation following photoexcitation of TiOPc is independently observed at both the P3HT/TiOPc and TiOPc/C_{60} interfaces using *FP*-TRMC, and the trilayer structure exhibits a strongly enhanced photoconductance signal-lifetime product relative to the bilayer controls, confirming that this structure serves to inhibit bimolecular recombination. Femtosecond TA evinces ultrafast hole and electron transfer as well as exciton-diffusion limited processes in each bilayer P3HT/TiOPc and TiOPc/C_{60}, respectively. In the P3HT/TiOPc bilayer, photoinduced hole transfer from TiOPc proceeds only for the crystalline domains of the polymer. In the P3HT/TiOPc/C_{60} trilayer, these results indicate that the initial charge-separated species are $P3HT^{\bullet+}/TiOPc^{\bullet-}$ and $TiOPc^{\bullet+}/C_{60}^{\bullet-}$ when TiOPc is selectively excited, and the final charge-separated product is $P3HT^{\bullet+}/TiOPc/C_{60}^{\bullet-}$, which is responsible for the long-lived photoconductance signals observed in *FP*-TRMC experiments on the trilayer.

EXPERIMENTAL SECTION

Materials and Instrumentation. Titanyl phthalocyanine (TiOPc) used in this work was obtained from two sources. An initial supply of sublimation-purified TiOPc was obtained from Prof. Erin Ratcliff at the University of Arizona. Subsequently, material was purchased from Aldrich and purified at NREL via three repetitions of temperature gradient sublimation, resulting in a purple powder consisting of needlelike crystals which sublime between 390 and 410 °C. RR-P3HT was obtained from Reike Metals (4002-EE; MW, average 50−70K; Lot no., PTL13-51) and used as received. C_{60} was obtained from Nano-C (98% purity) and used as received. Anhydrous chlorobenzene (98% purity) was purchased from Sigma-Aldrich and used as received. Electronic absorption spectra were recorded on a Varian 500 ultraviolet/visible/near-infrared (UV/vis/NIR) spectrophotometry system.

Thin-Film Preparation. Thin films of TiOPc, TiOPc/C_{60}, P3HT/TiOPc, and P3HT/TiOPc/C_{60} were prepared for *FP*-TRMC measurements as well as pump−probe transient absorption spectroscopy experiments. Thin films of RR-P3HT were coated onto quartz substrates by blade coating in a N_2 glovebox. Typical conditions were to use a 7.5 mg/mL solution of RR-P3HT in chlorobenzene, with solution and substrate temperature set to 40 °C. The bar was traversed at 15 mm/s with a 40 μm gap between the blade edge and the substrate. These conditions result in uniform P3HT films 30−50 nm thick. Deposition of TiOPc and C_{60} films was accomplished by vacuum sublimation in a thermal evaporator (Angstrom Engineering, Ontario, Canada) interfaced with an N_2 glovebox. Samples were coated with P3HT in a separate solvent box and transferred via a sealed transfer chamber to avoid any exposure to ambient atmosphere. Vacuum depositions were made at a typical base pressure of 8×10^{-7} Torr and at a rate for both materials of 0.5 Å/s. Temperature-controlled Radak crucibles were used in both cases, with deposition temperatures of ∼400 °C for TiOPc and 600 °C for C_{60}.

Flash-Photolysis Time-Resolved Microwave Conductivity Experiments. *FP*-TRMC measurements were carried out on a system that has been extensively described elsewhere.[34,36,42,43] Briefly, the sample is mounted and sealed into a microwave cavity in an N_2 glovebox and transferred to the experimental apparatus where ultrahigh purity N_2 flow through the cavity is maintained at all times to avoid any ambient exposure or photooxidation during the experiment. The sample is optically excited by a 4 ns fwhm laser pulse from an optical parametric oscillator (OPO, Continuum Panther), pumped by the 355 nm harmonic of an Nd:YAG laser (Continuum Powerlite), and sample photoconductance is measured by monitoring the transient change in microwave power absorption by the sample after the laser pulse.

Femtosecond Pump−Probe Transient Absorption Spectroscopy Experiments. Femtosecond transient absorption spectra were obtained using standard pump−probe methods (Ultrafast Systems, HELIOS, Sarasota, FL, United States). Optical pulses (<100 fs) centered at 800 nm are generated using a Ti:sapphire laser (Coherent, Libra, Santa Clara, CA, United States), which consists of a regenerative amplifier seeded by a mode-locked oscillator. The output of the regenerative amplifier is split to feed an optical parametric amplifier (Light Conversion Ltd., TOPAS-C, Vilnius, Lithuania), which generates excitation pulses tunable in wavelength from the UV through the NIR region. The pump beam is chopped at half the laser repetition rate (∼500 Hz). The polarization and attenuation of the pump beam are controlled by half-wave plate and polarizer pairs. The pump beam polarization is set to the parallel orientation with respect to the probe beam for these experiments. The pump beam is focused into the samples with an f = 50 cm lens, while the probe beam is focused with a concave mirror. The spot size diameter of the pump beam is ∼0.45 mm. The beam diameter is determined using the razor-blade method. The excitation pump pulse energy is measured using an energy meter (Ophir, Laserstar with PD10-pJ-C). A fraction (<0.3%) of the output from the regenerative amplifier is passed through an optical delay line and used to generate the white light continuum probe beam.

DOI: 10.1021/acs.jpcb.5b00110
J. Phys. Chem. B 2015, 119, 7729−7739

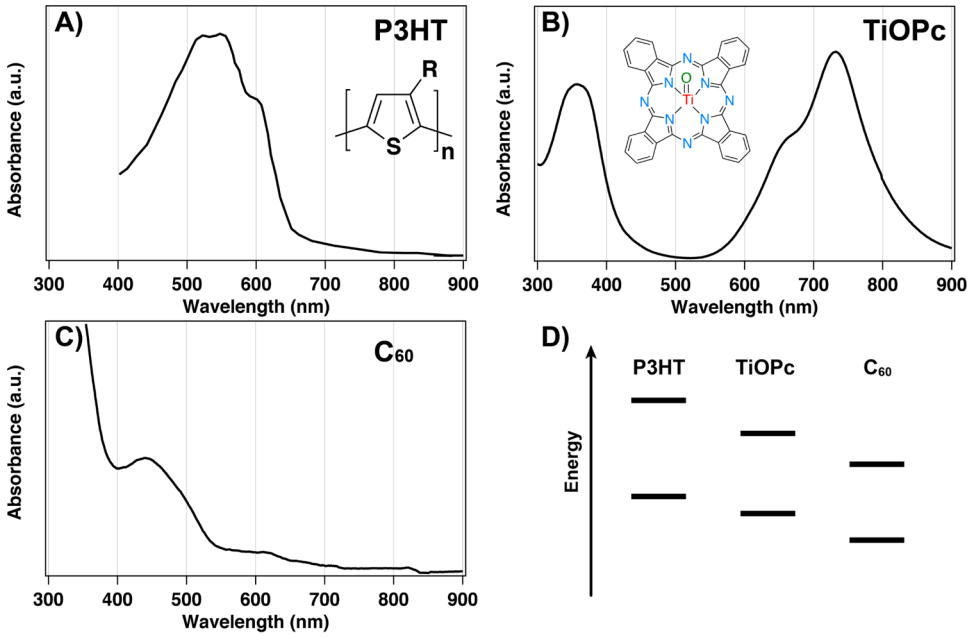

Figure 1. Molecular structures and thin-film electronic absorption spectra obtained for (A) P3HT (R = hexyl), (B) TiOPc, and (C) C_{60}. (D) Schematic energy levels for crystalline-RR-P3HT (solid line), TiOPc, and C_{60} depicting that crystalline-RR-P3HT/TiOPc and TiOPc/C_{60} form type-II heterostructures.

This white light continuum probe beam is split into two fractions before it passes through a sample, and one fraction is directed to a sample and a probe detector channel while the other fraction is directed to a reference detector channel. After passing through the sample, the probe light is adjusted using a variable neutral density filter and appropriate color glass filters to avoid saturating the detectors. Transient absorption data are recorded using a multichannel CMOS sensor and a multichannel InGaAs sensor for the 300−850 nm and 800−1500 nm regions, respectively. Pairs of consecutive spectra are measured with $I_{on}(\lambda)$ and $I_{off}(\lambda)$ to determine the difference spectrum, $\Delta A = \log I_{off}(\lambda)/I_{on}(\lambda)$. All these experiments utilize a quartz substrate; all transient optical studies are carried out at 20 ± 1 °C. All transient spectra reported represent averages obtained over 3−5 scans, with each scan consisting of 2000 frames with ∼200−500 data points. Following all pump−probe transient absorption experiments, electronic absorption spectra verified that the thin-film samples were robust.

Nanosecond−Microsecond Pump−Probe Transient Absorption Spectroscopy Experiments. Nanosecond−microsecond transient absorption spectra are obtained using an Ultrafast Systems EOS subnanosecond transient absorption spectrometer (Ultrafast Systems, EOS, Sarasota, FL, United States) that is housed within the Ultrafast Systems Helios femtosecond transient absorption spectrometer described above. The same pump beam as in femtosecond pump−probe transient absorption spectroscopy experiments is used. A depolarizer is used for a pump beam to compensate polarization dependence, and pump pulse energy is controlled using a variable neutral density filter. All transient optical studies are carried out at 20 ± 1 °C. All nanosecond−microsecond transient absorption spectra reported represent averages obtained for 60−120 min.

RESULTS AND DISCUSSION

The molecular structure of titanyl phthalocyanine (TiOPc) and electronic absorption spectra of thin films of neat components (P3HT, TiOPc, and C_{60}) are shown in Figure 1 along with a schematic energy level diagram, illustrating that crystalline-RR-P3HT/TiOPc and TiOPc/C_{60} form type-II heterostructures. Electronic absorption spectra of investigated multilayer thin-film samples are displayed in Figure 2A. Four thin-film sample configurations examined in this report are shown in Figure 2B, and the details of each thin-film preparation are described in the Experimental Section. In Figure 1B, the electronic absorption spectrum of neat TiOPc film (black) exhibits a Soret-band ($S_0 \rightarrow S_2$ transition) at around 350 nm, as well as Q-bands ($S_0 \rightarrow S_1$ transition) spanning from 600 to ∼850 nm, with peaks at ∼650 and 732 nm due to $Q_{0,1}$ and $Q_{0,0}$ transitions of TiOPc. These absorption features are characteristic of amorphous TiOPc films.[44−47] The similarity of the TiOPc Q-band absorption spectrum in all thin-film samples examined in

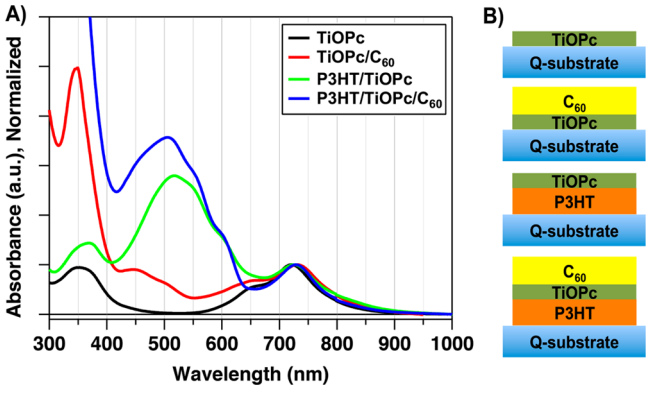

Figure 2. (A) Electronic absorption spectra of thin-film samples examined in this report: (black) TiOPc, (red) TiOPc/C_{60} bilayer, (green) P3HT/TiOPc bilayer, and (blue) P3HT/TiOPc/C_{60} trilayer. All spectra are displayed normalized to the maxima of TiOPc Q-band. (B) Four thin-film samples examined in this report. The details of thin-film preparation are described in the Experimental Section.

DOI: 10.1021/acs.jpcb.5b00110
J. Phys. Chem. B 2015, 119, 7729−7739

this study suggests (i) identical solid-phase morphology of TiOPc layers and (ii) a lack of ground-state interaction between TiOPc and C_{60} and/or P3HT. The electronic absorption spectrum (Figure 2A, blue) of the trilayer sample (P3HT/TiOPc/C_{60}) and the bilayer controls (Figure 2A, green and red for P3HT/TiOPc and TiOPc/C_{60}, respectively) each exhibit a linear combination of the individual components: (i) the absorption peak of C_{60} at ∼350 nm as well as weaker broad absorption structures tailing to ∼650 nm;[48−50] (ii) the broad absorption band of regioregular P3HT between 400 and 650 nm, which is characterized by a superposition of structureless absorption arising from the disordered polymer chains and a red-shifted vibronic progression that is characteristic of ordered chain segments that are electronically coupled;[43,51,52] and (iii) the previously described Soret and Q-bands of amorphous TiOPc.

Figure 3 shows flash-photolysis time-resolved microwave conductivity transients for each important combination of materials with selective excitation of the TiOPc layer. The *y*-axis ($\phi\Sigma\mu$) is the product of carrier generation yield and the sum of the carrier mobilities, calculated from the measured photoconductance, incident photon flux, and the absorptance of each sample. We describe the *FP*-TRMC experiment in the Experimental Section. We discuss the results for each sample in order of increasing complexity. The transients for the bilayers (green and yellow traces) show several interesting features as compared with the transients for the neat materials (blue trace for TiOPc; see Figure S1 in the Supporting Information for P3HT and C_{60}). In both cases (TiOPc/C_{60} and P3HT/TiOPc), we see a significant increase in $\phi\Sigma\mu$ for the bilayer over that observed when exciting either neat material, with a universal increase in the lifetime of the photoconductance signal when going from the neat materials to the bilayer. This is evidence of photoinduced charge transfer at both P3HT/TiOPc and TiOPc/C_{60} interfaces. However, the P3HT/TiOPc sample exhibits a slow (∼50 ns) rise component that is absent in all other transients.

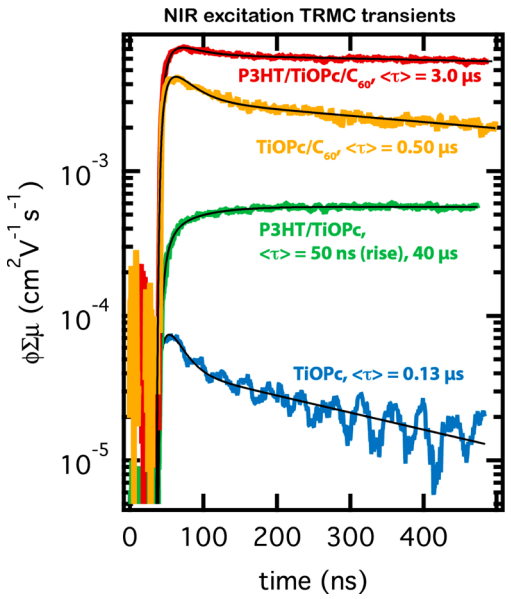

Figure 3. Time-resolved microwave photoconductance transients for NIR excitation (800 or 850 nm) of neat TiOPc (blue trace), P3HT/TiOPc (green trace), TiOPc/C_{60} (yellow trace), and P3HT/TiOPc/C_{60} (red trace). The *absorbed* excitation fluence in all cases was ∼0.6 μJ/cm^2, except for the neat TiOPc sample where 6.7 μJ/cm^2/pulse was required in order to obtain a measurable signal. The black lines are fits to a sum of up to two exponentials convoluted with the instrument response function. Average time constants from these fits for decay and in one case rise times are displayed in the trace labels.

The trilayer structure (P3HT/TiOPc/C_{60}, red trace) shows a signal that is greater than the linear combination of that observed for each bilayer with a lifetime that is intermediate between those observed for each bilayer. (See Figure S1 in the Supporting Information for data measured with other excitation wavelengths and additional control experiments.) Two of these observations are particularly curious: the slow rise component in the photoconductance of the P3HT/TiOPc sample and the superlinear increase in signal observed when moving from the bilayer (P3HT/TiOPc and TiOPc/C_{60}) to trilayer (P3HT/TiOPc/C_{60}) structures.

The transient for the P3HT/TiOPc bilayer (green trace) is best fit by a biexponential having a rise component of 50 ns and a decay time-constant of 40 μs. As the absorption spectrum of the TiOPc film evinces mostly amorphous-like features, it is possible that trapped excitons or charge-separated pairs ($TiOPc^{\bullet+}$/$TiOPc^{\bullet-}$) in the TiOPc layer contribute to the slow rise component observed for the P3HT/TiOPc bilayer, and this hypothesis is consistent with transient absorption spectroscopy results discussed below. The absence of this feature in the TiOPc/C_{60} bilayer and the P3HT/TiOPc/C_{60} trilayer is likely simply a matter of relative magnitude: only the P3HT/TiOPc bilayer has a carrier yield low enough for this contribution to be observable.

The second interesting point is that the photoconductance signal observed in the trilayer structure is greater than the linear combination of that observed for the two bilayers. In P3HT/TiOPc/C_{60}, two exciton-dissociating interfaces are present: between P3HT/TiOPc and TiOPc/C_{60}. If the photoconductance signal is solely determined by charge carrier yield, one would expect that the photoconductance of the trilayer structure would be the sum of the photoconductance observed for each bilayer individually, assuming the two interfaces do not compete for the same excitons. Thus, the superlinear increase in the photoconductance (red trace in Figure 3) of the trilayer (P3HT/TiOPc/C_{60}) relative to the individual bilayers (P3HT/TiOPc and TiOPc/C_{60}) is puzzling at first. However, it is important to remember that the photoconductance signal is governed not merely by the carrier yield (ϕ) but also by the local gigahertz mobility ($\Sigma\mu$). If charges generated in a low-mobility material (such as TiOPc) are ultimately transferred to a higher-mobility material (such as C_{60}), the overall photoconductance will be enhanced, even for a constant yield.

In the present case, only the gigahertz hole mobility in P3HT is known: 0.014 cm^2 V^{-1} s^{-1}.[41,53] Using this value we can estimate the yield of charges for the neat P3HT sample in Figure S1 in the Supporting Information as ∼0.7%. Furthermore, if we assume that the electron mobility in TiOPc is small relative to the hole mobility in the polymer, we estimate the charge yield in the P3HT/TiOPc bilayer for 800 nm excitation to be ≤4%. The significance of the assumption above is that 4% is the upper limit for the carrier yield in the P3HT/TiOPc bilayer under the conditions of the measurement in Figure 3. It is important to note here that the gigahertz frequency mobility, particularly in polymers, is quite different from that observed through bulk quasi DC methods. The gigahertz frequency hole mobility in P3HT has been shown to be remarkably insensitive to variations in molecular order and

DOI: 10.1021/acs.jpcb.5b00110
J. Phys. Chem. B 2015, 119, 7729−7739

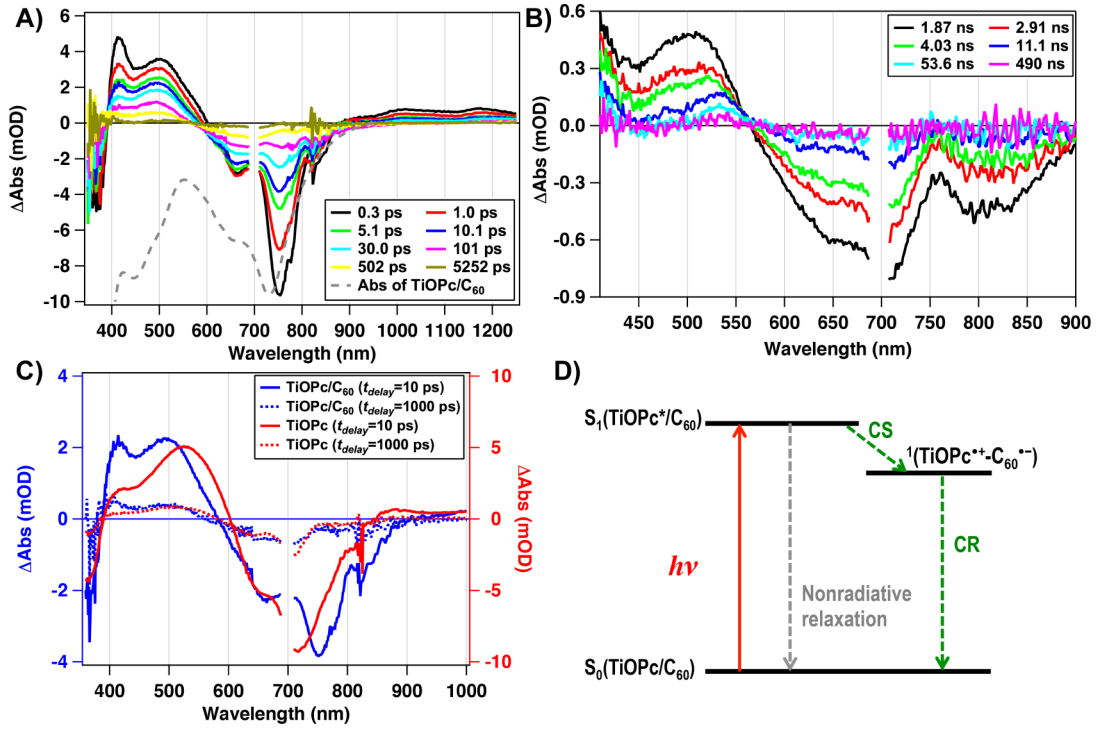

Figure 4. Representative vis−NIR transient absorption spectra of the TiOPc/C_{60} bilayer from (A) fsTA (an inversed ground-state absorption spectrum is displayed for comparison) and (B) nsTA spectroscopy, recorded at pump−probe time delays noted. (C) Comparative femtosecond vis−NIR transient absorption spectra obtained for (blue) TiOPc/C_{60} and (red) TiOPc at same pump−probe time delays noted for comparison. (D) A schematic diagram depicting photoinduced electron-transfer process on TiOPc/C_{60} following exclusive photoexcitation on the TiOPc layer. Experimental conditions: λ_{ex} = 700 nm; temperature = 20 °C; parallel polarization; excitation pump fluence = 90−300 and ∼600 μJ/cm^2 for fsTA and nsTA spectroscopy, respectively.

microstructure, even when orders-of-magnitude changes are observed in bulk carrier mobility.[43,54] Only for extreme cases, such as comprehensive alignment of the polymer chains, is the gigahertz mobility affected.[55] In the present study all the P3HT layers were prepared identically, and any small variations in microstructure between samples is very unlikely to affect our results.

For samples containing C_{60}, it is the electron mobility in the fullerene that dominates the signal. While the precise value is not known, it has been commonly observed that the gigahertz frequency electron mobility in fullerene derivatives is typically much larger than the hole mobility in P3HT, on the order of 0.1 cm^2 V^{-1} s^{-1}.[56−58] This explains why the $\phi\Sigma\mu$ for the TiOPc/C_{60} bilayer is an order of magnitude larger than that for the P3HT/TiOPc bilayer and also explains the superlinear increase in signal when the trialyer is formed: electrons generated at the TiOPc/P3HT interface migrate across the TiOPc layer and are transferred to the C_{60}. When this occurs, their contribution to the signal is dramatically increased. If we assume that this transfer is 100% efficient, it provides us with a simple way to estimate the gigahertz electron mobility in the C_{60} layer and thus the total yield in the trilayer system. If the difference in signal between the TiOPc/C_{60} bilayer and the trilayer is solely due to an additional yield of 4%, then the mobility of electrons in the C_{60} may be calculated as

$$\sum \mu_{C_{60}} = \frac{(\phi \sum \mu)_{\mathrm{P3HT/TiOPc/C_{60}}} - (\phi \sum \mu)_{\mathrm{TiOPc/C_{60}}}}{\phi_{\mathrm{P3HT/TiOPc}}} = 0.06 \text{ cm}^2 \text{ V}^{-1} \text{ s}^{-1}$$

This number gives a lower-limit for the gigahertz electron mobility in a film of C_{60} and is qualitatively consistent with previous estimates.[56−58] Using this number for the electron mobility in the C_{60} layer, we can calculate the yield for the TiOPc/C_{60} bilayer in Figure 3 as ≤15% and the ultimate yield of the trilayer at low light intensities (0.1 μJ/cm^2) as ≤28%. These are quite small numbers for the estimated yield of free charges, especially given the small thickness of the TiOPc layer that is being directly excited (at 800 nm). This result implies a short exciton diffusion length in the TiOPc film, a low exciton dissociation efficiency, and/or fast geminate recombination at both interfaces. This value for the charge separation efficiency for as-deposited (amorphous) TiOPc is consistent with previous results on TiOPc/C_{60} devices.[33]

To examine the detailed excited-state dynamics of the P3HT/TiOPc/C_{60} trilayer such as charge generation dynamics and the origin of photoconductance, pump−probe transient absorption spectroscopy was employed. Figures 4, 5, and 6 display representative transient absorption (TA) spectra obtained for thin-film samples of TiOPc/C_{60}, P3HT/TiOPc, and P3HT/TiOPc/C_{60}, respectively. With an excitation wavelength of 700 nm, we can selectively excite the TiOPc layer as in our *FP*-TRMC measurements. TA spectra of neat TiOPc at $t_{delay} \approx 0.3$ ps show (i) negative difference absorbance signals (ΔAbs) near 370, 650, and 739 nm originating from $S_0 \rightarrow S_1$ ($Q_{0,1}$ and $Q_{0,0}$ transition) and $S_0 \rightarrow S_2$ ground-state bleaching (GSB) as a result of depleted ground-state population and stimulated emission and (ii) positive TA bands peaking at 424 and ∼540 nm (Figure S2 in the Supporting Information). These results are consistent with previous transient absorption spectroscopy studies of TiOPc

DOI: 10.1021/acs.jpcb.5b00110
J. Phys. Chem. B 2015, 119, 7729−7739

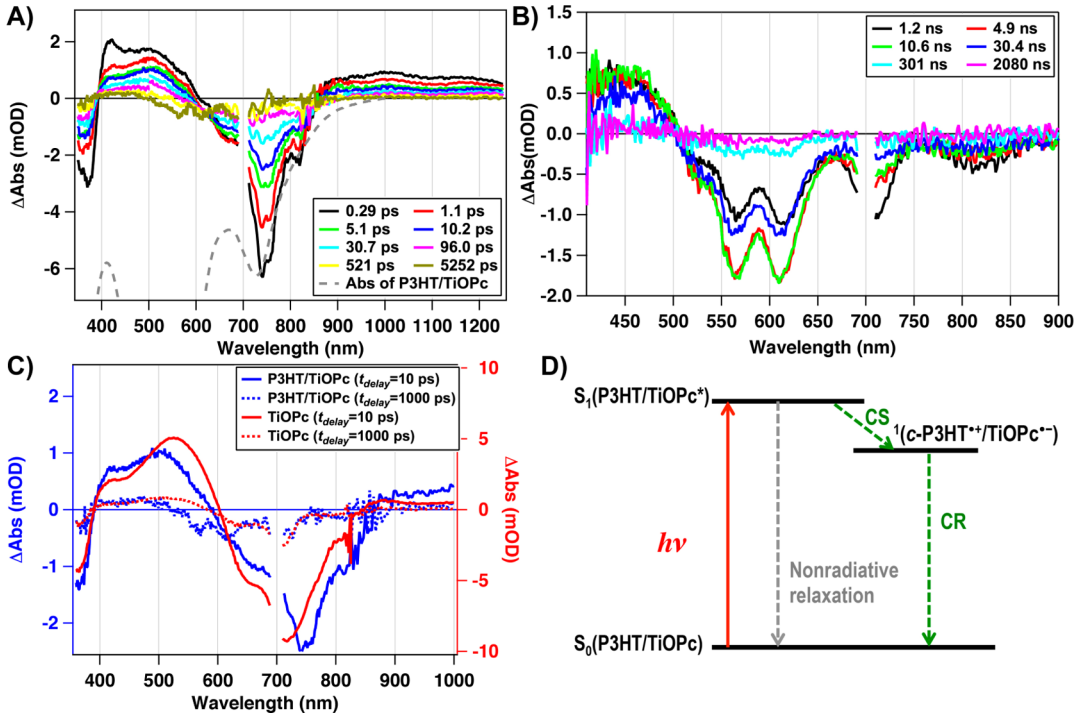

Figure 5. Representative vis−NIR transient absorption spectra of the P3HT/TiOPc bilayer from (A) fsTA (an inversed ground-state absorption spectrum is displayed for comparison) and (B) nsTA spectroscopy, recorded at pump−probe time delays noted. (C) Comparative femtosecond vis−NIR transient absorption spectra obtained for (blue) P3HT/TiOPc and (red) TiOPc at same pump−probe time delays noted for comparison. (D) A schematic diagram depicting photoinduced hole-transfer process on P3HT/TiOPc following exclusive photoexcitation on the TiOPc layer. *c*-P3HT stands for H-aggregate domain in the P3HT layer. Experimental conditions: λ_{ex} = 700 nm; temperature = 20 °C; parallel polarization; excitation pump fluence = 90−300 and ∼600 μJ/cm^2 for fsTA and nsTA spectroscopy, respectively.

films as well as structurally similar phthalocyanines; therefore, TA features peaking at 424 and ∼540 nm in 0.3 ps < t_{delay} < 100 ps can represent spectral signatures of ^{1}TiOPc*.[45,59,60] The multiwavelength global analysis yielded time constants of 0.7 ps, 8 ps, 82 ps, and 4.8 ns using a multiexponential function; the 4.8 ns time constant is assigned to the intrinsic singlet-state exciton lifetime of TiOPc, as this is consistent with the fluorescence lifetime of TiOPc in solution.[60]

As in TRMC, the excited-state dynamics at the interface between TiOPc/C_{60} and P3HT/TiOPc were studied separately in bilayer films using transient absorption spectroscopy (Figures 4 and 5). In transient absorption spectra of TiOPc/C_{60} (Figure 4A), new positive peaks at 417 and 500 nm at t_{delay} ≈ 0.3 ps are evident in addition to the GSB bands in neat TiOPc (Figure S2 in the Supporting Information). Note that although the typical spectral signature of the C_{60} radical anion is expected at ∼1080 nm, it is largely buried under broad NIR TA bands because of its low extinction coefficient (ε of $C_{60}^{\bullet-}$ ≈ 12 000 M^{-1} cm^{-1}, in benzonitrile);[61−63] the transient absorption spectrum of TiOPc/C_{60} in the visible spectral domain at 0.3 ps < t_{delay} < 5 ns clearly contrasts with that of ^{1}TiOPc* (Figure 4C and Figure S2 in the Supporting Information). Previous studies of phthalocyanines have established the absorption spectra of phthalocyanine radical cations, which evince peaks at 420 and 520−540 nm;[59,64,65] therefore, from these transient absorption data, we conclude that the selective photoexcitation on the TiOPc layer exhibits photoinduced electron transfer from TiOPc to C_{60} to generate (TiOPc$^{\bullet+}$—$C_{60}^{\bullet-}$). In Figure 4B, nsTA spectra recorded up to ∼500 ns time delay show that these transient species (TiOPc$^{\bullet+}$—$C_{60}^{\bullet-}$) exist even after 50 ns, and the charge recombination time constants of 4.5 and 366 ns determined from multiwavelength global analysis in Figure S3A in the Supporting Information agree with the time constant of ∼6.4 and 470 ns extracted from a double exponential fit of the *FP*-TRMC transient at similar though somewhat lower fluence (600 μJ/cm^2 in TA vs 300 μJ/cm^2 in TRMC; Figure S5 in the Supporting Information). These combined *FP*-TRMC and TA results unambiguously show that the photoinduced carriers (TiOPc$^{\bullet+}$—$C_{60}^{\bullet-}$) are responsible for long-lived excited-state species, as summarized in Figure 4D.

On the other hand, in the transient absorption spectra of the P3HT/TiOPc bilayer, positive bands are evident at ∼420 and 500 nm at t_{delay}≈ 0.3 ps, and structured GSB bands of P3HT are emerging at 565 and 615 nm, as evident at t_{delay}> 500 ps (Figure 5A−C), which indicate the depletion of P3HT ground-state population for the generation of either excitons or polarons. Considering the $S_0 \rightarrow S_1$ absorption peak of P3HT absorption at 615 nm and the $S_0 \rightarrow S_1$ absorption peak of TiOPc at 732 nm, energy transfer from ^{1}TiOPc* to P3HT can be excluded. The lack of P3HT exciton transient absorption band, which has been reported to appear at ∼1200 nm,[7,66−70] confirms this assumption and is consistent with our results for 550 nm direct excitation of P3HT (Figure S4A in the Supporting Information). A plausible explanation is that following photoexcitation on TiOPc, three competing processes occur from ^{1}TiOPc*: (i) ultrafast hole transfer from a small portion of ^{1}TiOPc* to P3HT, located near the interface or penetrated into the polymer layer, occurs and produces (P3HT$^{\bullet+}$—TiOPc$^{\bullet-}$); (ii) a decay of ^{1}TiOPc* to the ground-state; and (iii) ^{1}TiOPc* exciton diffusion to the TiOPc/P3HT interface. Following the ultrafast process, the P3HT GSB continues to grow within the 5.2 ns time window

DOI: 10.1021/acs.jpcb.5b00110
J. Phys. Chem. B 2015, 119, 7729−7739

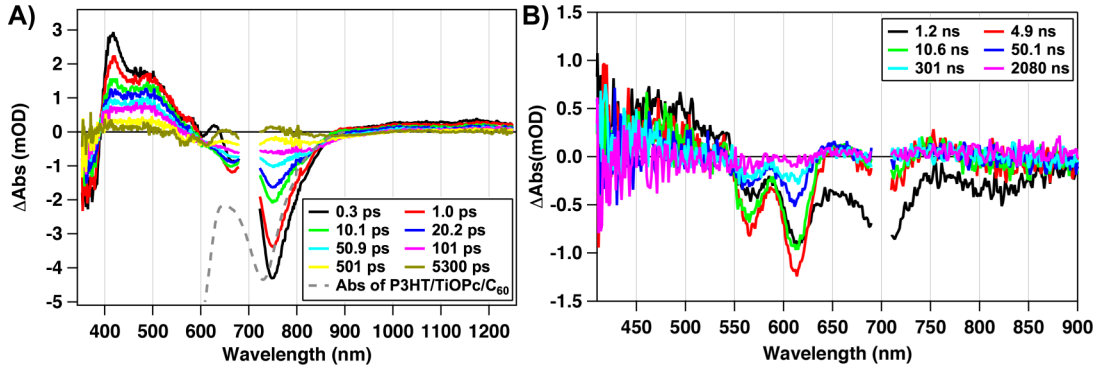

Figure 6. Representative vis−NIR transient absorption spectra of the P3HT/TiOPc/C_{60} trilayer from (A) fsTA (an inversed ground-state absorption spectrum is displayed for comparison) and (B) nsTA spectroscopy, recorded at the pump−probe time delays noted. Experimental conditions: λ_{ex} = 700 nm; temperature = 20 °C; parallel polarization; excitation pump fluence = 90−300 and ∼600 μJ/cm^2 for fsTA and nsTA spectroscopy, respectively.

and suggests that exciton diffusion-limited hole transfer also occurs. Fits to the transient signal at 565 and 615 nm show a rise time constant of 2 ns; therefore, this exciton diffusion-limited hole-transfer process completes in <10 ns (Figure S3B in the Supporting Information). Furthermore, it should be noted that the GSB band attributed to P3HT evinces features only from the structured red-edge of its electronic absorption spectrum. According to the model proposed by Spano et al. to explain the electronic absorption spectrum of RR-P3HT, these features at 565 and 615 nm arise from the formation of weakly coupled H-aggregates. The broad absorption at 500 nm expected for amorphous P3HT is absent from the GSB.[43,71,72] A TA spectrum of P3HT/TiOPc with 550 nm excitation obtained at t_{delay} = 0.3 ps represents ^{1}P3HT* exciton spectral signatures, and as a result, the ground states of both amorphous and H-aggregated P3HT domain are depleted (Figure S4A in the Supporting Information). Hence, the GSB in TA spectrum with 550 nm shows contributions from both amorphous and H-aggregated P3HT domain. On the other hand, with 700 nm excitation, no direct excitons would be generated in the P3HT domain. Instead, ground-state depletion in the P3HT occurs only in the domains involved in photoinduced hole transfer with TiOPc to produce P3HT$^{\bullet+}$/TiOPc$^{\bullet-}$. The data suggests that only H-aggregated species participate in photoinduced hole-transfer processes with TiOPc, whereas electron transfer proceeds from P3HT to TiOPc whether the initial excitation is on an H-aggregate or not. It is well-established that polymer bandgaps can vary depending on the local microstructure,[73,74] and recently Sweetnam et al. reported the difference in valence band energy between aggregated and disordered P3HT to be 150 meV.[14] Therefore, we suggest that photoinduced hole transfer between P3HT and TiOPc is mediated by the raised valence band energy (relative to vacuum) in H-aggregated P3HT domains. We compared the energetic driving force (ΔE_{CS}) for charge generation of amorphous P3HT/TiOPc and H-aggregated P3HT/TiOPc using the following equation:[74]

$$\Delta E_{CS} = (\mathrm{IP} - \mathrm{EA}) - E_S \quad (1)$$

where IP is the ionization potential of the donor (P3HT), EA the electron affinity of the acceptor (TiOPc), and E_S the energy of photoexcited singlet-state exciton of TiOPc as we excite the TiOPc layer. We use the previous literature values of 4.95 and 4.8 eV for the amorphous and H-aggregate domain P3HT IPs, respectively,[14,75] and 1.28 eV for E_S of TiOPc from the absorption onset energy of TiOPc in Figure 1B. As TiOPc EA is not available at the same conditions, to the best of our knowledge, instead we use a TiOPc IP of 5.2 eV from UV photoelectron spectroscopy[33] and an electrochemical bandgap of 1.57 eV obtained from cyclic voltammetry[76] to determine a TiOPc EA of 3.63 eV. From these parameters, ΔE_{CS} is calculated as 0.04 eV and −0.11 eV for the amorphous P3HT/TiOPc and H-aggregate P3HT/TiOPc, respectively, suggesting substantially reduced ΔE_{CS} for the amorphous P3HT/TiOPc.

In previous reports, a pronounced, broad, positive NIR TA band peaking at ∼1000 nm has been assigned to P3HT positive polarons[7,66,68,69] as well as a TA signal in the vicinity of ∼650 nm.[66] This broad NIR TA band at ∼1000 nm appears with 550 nm excitation, but is lacking with 700 nm excitation (Figure S4A in the Supporting Information). Presumably, the NIR TA band represents polarons in disordered P3HT chains. The TA band near 650 nm is discernable for both 700 and 550 nm excitation, though it overlaps strongly with the GSB of TiOPc and P3HT, making it appear as a minimum in the GSB signal when compared between Figures 4B and 5B (also, see Figure S4 in our Supporting Information). We suggest that this difference in TA spectra is due to differing spectral signatures of polarons in the H-aggregate P3HT domain versus that in isolated chains and is consistent with the previous literature results that compare delocalized (2D) polarons in RR-P3HT to 1D polarons on isolated chains.[77,78] Figure 5B presents TA spectra for P3HT/TiOPc recorded from 1 ns to 10 μs time domain. Again, the TA spectra at t_{delay}≈ 6.6 ns unambiguously exhibit a rise of H-aggregate P3HT GSB bands, which confirms delayed diffusion-controlled hole transfer, and this exciton diffusion-limited hole transfer competes with exciton decay of TiOPc to the ground state as probed by the decay of the TiOPc GSB signals. However, this charge-separated state persists for more than 1 μs, which is substantially longer-lived than the charge-separated state (τ_{CR} ≈ 4.5 and 370 ns) in TiOPc/C_{60}. Multiwavelength global analysis determined the time constants for charge recombination, τ_{CR}, to be 45 and 1200 ns (Figure S3B in the Supporting Information). This biphasic transient decay contrasts with the decay dynamics measured via *FP*-TRMC at a similar excitation density (Figure S5 in the Supporting Information). This apparent disagreement is caused by the fact that the transient absorption measurement provides a signal proportional to the sum of all excited-state species in the P3HT/TiOPc film, whereas in *FP*-TRMC only mobile charges are probed. Thus, the 45 ns decay component of the

DOI: 10.1021/acs.jpcb.5b00110
J. Phys. Chem. B 2015, 119, 7729−7739

GSB may be associated with geminate recombination of trapped charges at the interface (or CT states), which are invisible to the TRMC measurements. Previous studies of neat P3HT as well as P3HT:PCBM blend systems observed complication of carrier dynamics due to multiple competing processes such as hole−dark carrier annihilation and carrier trapping−detrapping in P3HT domain over the nanosecond time domain.[8,43] Over the 10 μs time domain, we do not observe any evidence of hole transfer from the H-aggregate P3HT domain to disordered P3HT domains, which is consistent with previous literature that probed the absence of energetic overlap of valence bands between amorphous and ordered P3HT domains.[73] These photoinduced hole-transfer results between P3HT and TiOPc summarized in Figure 5D highlight the significance of understanding the correlation between morphological microstructures and photoinduced dynamics.

Lastly, the transient absorption spectra of the P3HT/TiOPc/C_{60} trilayer (Figure 6) exhibit combined spectral features of each of the TiOPc/C_{60} and the P3HT/TiOPc bilayers. Following photoexcitation, instantaneous positive peaks at 417 and 500 nm at $t_{delay} \approx 0.3$ ps due to characteristic TiOPc radical cations and anions are evident as well as GSB bands of TiOPc near 370 and ∼730 nm. In addition, GSB bands of P3HT at ∼565 and ∼615 nm are observed to overlap with the above-mentioned positive TA bands of TiOPc radical species. These structured GSB bands again originate from H-aggregate P3HT as in P3HT/TiOPc as described above. Our TA data lacks the transient absorption signature (∼1200 nm) of the P3HT exciton, which excludes energy transfer from TiOPc to P3HT. Transient absorption spectra at $t_{delay} \approx 0.3$ ps featuring characteristic TiOPc radical cations and anions indicate ultrafast charge generation, which is consistent with the bilayer results in Figures 4A and 5A followed by the exciton diffusion-controlled charge generation. Similar to the spectral evolution of the transient absorption features in the P3HT/TiOPc bilayer, a growth of P3HT GSB bands was noted within the ∼5 ns time domain, as shown in Figure 6. In Figure 7, the dynamics of the ground-state bleach signal for TiOPc is compared between the two bilayers and the trilayer. In a P3HT/TiOPc/C_{60} trilayer, the GSB band decays ∼89% during ∼10 ns. In contrast, the GSB recovery of TiOPc in the bilayers (P3HT/TiOPc or TiOPc/C_{60}) is much slower, with a significant long-lived component that persists after 30 ns. The GSB recovery of TiOPc and the decay of TiOPc radical transient absorption in the P3HT/TiOPc/C_{60} sample is best fit with biphasic exponential decay with time constants of 2 and 11 ns (Figure S3C in the Supporting Information). We assign this fast decay of the TiOPc TA to diffusion of charges in the TiOPc and subsequent secondary charge transfer at each interface, where holes are transferred into the P3HT and electrons are transferred into C_{60}. Additionally, recombination may take place in the TiOPc layer as electrons and holes diffuse from the two different interfaces at which they are generated.

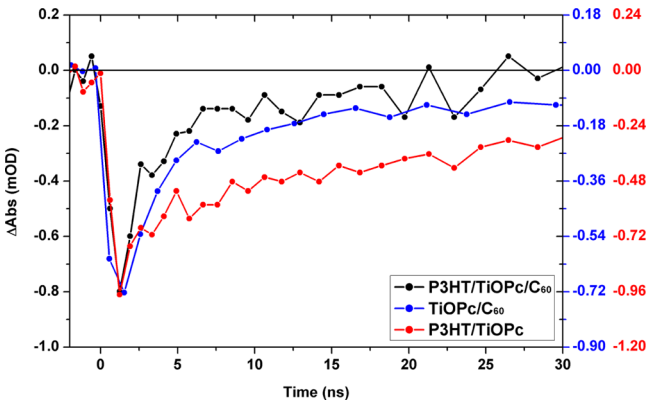

Figure 7. Comparative normalized ground-state bleaching signals at a probe wavelength, λ_{pr} = 715 nm, obtained for P3HT/TiOPc/C_{60} (black, left y-axis), TiOPc/C_{60} (blue, right y-axis), and P3HT/TiOPc (red, right y-axis) with dominant excitation on TiOPc. Experimental conditions: λ_{ex} = 700 nm; excitation pump fluence = ∼600 μJ/cm^2; temperature = 20 °C.

The evolution of the TA spectra as well as *FP*-TRMC transients for the P3HT/TiOPc/C_{60} trilayer strongly suggest that the charge separation in P3HT/TiOPc/C_{60} produces a final charge-separated product of (P3HT$^{\bullet+}$/TiOPc/$C_{60}^{\bullet-}$) from (P3HT/TiOPc*/C_{60}) via electron-transfer and hole-transfer processes. Multiwavelength global analysis determined the time constants for charge recombination, τ_{CR}, to be 11, 99, and 1600 ns, in good agreement with those derived from TRMC transients: 11 ns and 1.2 μs (Figures S3C and S5 in the Supporting Information). An additional 99 ns decay time constant possibly derives from trapped polaron decay in the P3HT layer, because this time constant appears only in the recovery GSB of the H-aggregate of the P3HT. Figure 8 summarizes photoinduced electron/hole-transfer and charge recombination processes in the P3HT/TiOPc/C_{60} trilayer following photoexcitation of the TiOPc layer. Following photoexcitation of TiOPc, electron/hole transfer occurs at either P3HT/TiOPc or TiOPc/C_{60} interfaces. At the P3HT/TiOPc interface, only H-aggregate P3HT domains interact with the excited TiOPc layer to produce P3HT$^{\bullet+}$/TiOPc$^{\bullet-}$, and no further interactions between H-aggregate P3HT and disordered P3HT are observed. The carriers associated with the TiOPc$^{\bullet+}$ and TiOPc$^{\bullet-}$ species that are produced at the TiOPc/C_{60} and P3HT/TiOPc interfaces, respectively, migrate to the opposite interface to produce P3HT$^{\bullet+}$/TiOPc/$C_{60}^{\bullet-}$ and compete with recombination within the TiOPc layer itself.

CONCLUSIONS

We combined flash-photolysis time-resolved microwave conductivity experiments (*FP*-TRMC) and femtosecond−nanosecond pump−probe transient absorption spectroscopy to investigate photoinduced carrier generation and recombination dynamics of ternary cascade heterojunction (P3HT/TiOPc/C_{60}) composed of poly(3-hexylthiophene), titanyl phthalocyanine, and fullerene. Carrier generation following photoexcitation on the TiOPc layer is independently observed at both the P3HT/TiOPc and TiOPc/C_{60} interfaces, and the trilayer P3HT/TiOPc/C_{60} structure exhibits enhanced photoconductance−lifetime product relative to the bilayer controls. From *FP*-TRMC of bilayer samples (P3HT/TiOPc and TiOPc/C_{60}) with photoexciting the TiOPc layer, we see a yield-mobility product ($\phi\Sigma\mu$) significantly larger than the linear combination of $\phi\Sigma\mu$ for each of the neat materials, and the dynamics evinced a universal increase in the lifetime of the photoconductance signal when going from the individual neat materials to the two bilayer structures. This shows that photoinduced charge transfer occurs at both the P3HT/TiOPc and TiOPc/C_{60} interfaces. Furthermore, $\phi\Sigma\mu$ of the trilayer (P3HT/TiOPc/C_{60}), which exceeds the sum of $\phi\Sigma\mu$ from each separate bilayer (P3HT/TiOPc and TiOPc/C_{60}),

DOI: 10.1021/acs.jpcb.5b00110
J. Phys. Chem. B 2015, 119, 7729−7739

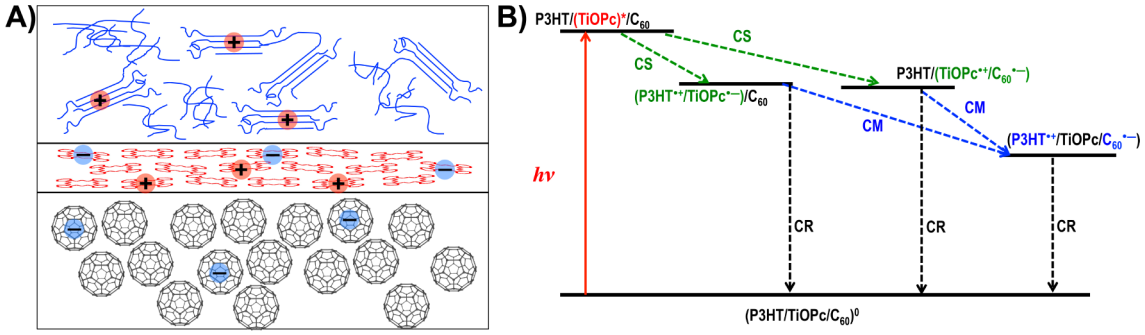

Figure 8. Illustration of photoinduced hole- and electron-transfer processes on P3HT/TiOPc/C_{60} following exclusive photoexcitation on TiOPc. For visual simplicity, intermediate charge-transfer states are omitted. (CS, charge separation; CM, charge migration; CR, charge recombination).

suggests that carriers from one interface interact with the opposite interface. Under our assumption that the migration of carriers to the other interface is 100% efficient at low excitation fluence conditions, the lower limit of the electron mobility in the C_{60} is determined to be ~0.06 $cm^2 V^{-1} s^{-1}$, a value that agrees well with previous literature values. From pump−probe transient absorption spectroscopy, more detailed carrier generation dynamics were studied on a faster time scale. Following photoexcitation exclusively of the TiOPc layer using a NIR wavelength, the trilayer P3HT/TiOPc/C_{60} sample probed carrier generation through hole- and electron-transfer processes at the interfaces of P3HT/TiOPc and TiOPc/C_{60}, respectively. Each bilayer, P3HT/TiOPc and TiOPc/C_{60}, exhibited ultrafast electron/hole transfer as well as exciton diffusion-limited processes. Our pump−probe transient absorption results also indicate that following initial charge generation processes to produce $P3HT^{\bullet+}$/$TiOPc^{\bullet-}$ and $TiOPc^{\bullet+}/C_{60}^{\bullet-}$ at each interface from (P3HT/TiOPc*/C_{60}) via electron-transfer and hole-transfer processes, the final charge-separated product of ($P3HT^{\bullet+}$/TiOPc/$C_{60}^{\bullet-}$) is responsible for the long-lived photoconductance signals at *FP*-TRMC. At the TiOPc/P3HT interfaces in both P3HT/TiOPc and P3HT/TiOPc/C_{60} samples, electron transfer appears to occur only with the crystalline (weakly coupled H-aggregate) phase of the P3HT.

We have demonstrated that the combination of *FP*-TRMC and classic pump−probe transient absorption spectroscopy can serve to complement each other and can be utilized to elaborate charge generation and recombination dynamics for more complicated ternary cascade heterojunction systems.

■ ASSOCIATED CONTENT

Supporting Information

Additional thin-film electronic absorption and transient spectroscopic experimental data. The Supporting Information is available free of charge on the ACS Publications website at DOI: 10.1021/acs.jpcb.5b00110.

■ AUTHOR INFORMATION

Corresponding Author

*E-mail: garry.rumbles@nrel.gov.

Notes

The authors declare no competing financial interest.

■ ACKNOWLEDGMENTS

We thank Prof. Erin Ratcliff at the University of Arizona for supplying the initial TiOPc sample. The experimental development of the multilayer systems was supported by the Laboratory Directed Research and Development (LDRD) Program at the National Renewable Energy Laboratory under Task 06RF1201. The flash-photolysis transient microwave (*FP*-TRMC) and femtosecond−nanosecond pump−probe transient absorption (fsTA and nsTA) spectroscopic studies were supported by the Solar Photochemistry Program, Division of Chemical Sciences, Geosciences, and Biosciences, Office of Basic Energy Sciences, U.S. Department of Energy. This work was supported by the U.S. Department of Energy under Contract DE-AC36-08-GO28308 with the National Renewable Energy Laboratory.

■ REFERENCES

(1) Yu, G.; Gao, J.; Hummelen, J. C.; Wudl, F.; Heeger, A. J. Polymer Photovoltaic Cells: Enhanced Efficiencies via a Network of Internal Donor-Acceptor Heterojunctions. *Science* **1995**, *270*, 1789−1791.

(2) Brédas, J.-L.; Norton, J. E.; Cornil, J.; Coropceanu, V. Molecular Understanding of Organic Solar Cells: The Challenges. *Acc. Chem. Res.* **2009**, *42*, 1691−1699.

(3) Zhu, X.-Y.; Yang, Q.; Muntwiler, M. Charge-Transfer Excitons at Organic Semiconductor Surfaces and Interfaces. *Acc. Chem. Res.* **2009**, *42*, 1779−1787.

(4) Cheng, Y.-J.; Yang, S.-H.; Hsu, C.-S. Synthesis of Conjugated Polymers for Organic Solar Cell Applications. *Chem. Rev. (Washingtong, DC, U.S.)* **2009**, *109*, 5868−5923.

(5) Clarke, T. M.; Durrant, J. R. Charge Photogeneration in Organic Solar Cells. *Chem. Rev. (Washingtong, DC, U.S.)* **2010**, *110*, 6736−6767.

(6) Deibel, C.; Strobel, T.; Dyakonov, V. Role of the Charge Transfer State in Organic Donor-Acceptor Solar Cells. *Adv. Mater. (Weinheim, Ger.)* **2010**, *22*, 4097−4111.

(7) Howard, I. A.; Mauer, R.; Meister, M.; Laquai, F. Effect of Morphology on Ultrafast Free Carrier Generation in Polythiophene: Fullerene Organic Solar Cells. *J. Am. Chem. Soc.* **2010**, *132*, 14866−14876.

(8) Ferguson, A. J.; Kopidakis, N.; Shaheen, S. E.; Rumbles, G. Dark Carriers, Trapping, and Activation Control of Carrier Recombination in Neat P3HT and P3HT:PCBM Blends. *J. Phys. Chem. C* **2011**, *115*, 23134−23148.

(9) Coffey, D. C.; Larson, B. W.; Hains, A. W.; Whitaker, J. B.; Kopidakis, N.; Boltalina, O. V.; Strauss, S. H.; Rumbles, G. An Optimal Driving Force for Converting Excitons Into Free Carriers in Excitonic Solar Cells. *J. Phys. Chem. C* **2012**, *116*, 8916−8923.

(10) Bakulin, A. A.; Rao, A.; Pavelyev, V. G.; van Loosdrecht, P. H. M.; Pshenichnikov, M. S.; Niedzialek, D.; Cornil, J.; Beljonne, D.; Friend, R. H. The Role of Driving Energy and Delocalized States for Charge Separation in Organic Semiconductors. *Science* **2012**, *335*, 1340−1344.

(11) Grancini, G.; Maiuri, M.; Fazzi, D.; Petrozza, A.; Egelhaaf, H.-J.; Brida, D.; Cerullo, G.; Lanzani, G. Hot Exciton Dissociation in Polymer Solar Cells. *Nat. Mater.* **2013**, *12*, 29−33.

DOI: 10.1021/acs.jpcb.5b00110
J. Phys. Chem. B 2015, 119, 7729−7739

(12) Reid, O. G.; Pensack, R. D.; Song, Y.; Scholes, G. D.; Rumbles, G. Charge Photogeneration in Neat Conjugated Polymers. *Chem. Mater.* **2014**, *26*, 561−575.
(13) Vandewal, K.; Albrecht, S.; Hoke, E. T.; Graham, K. R.; Widmer, J.; Douglas, J. D.; Schubert, M.; Mateker, W. R.; Bloking, J. T.; Burkhard, G. F.; et al. Efficient Charge Generation by Relaxed Charge-Transfer States at Organic Interfaces. *Nat. Mater.* **2014**, *13*, 63−68.
(14) Sweetnam, S.; Graham, K. R.; Ngongang Ndjawa, G. O.; Heumüller, T.; Bartelt, J. A.; Burke, T. M.; Li, W.; You, W.; Amassian, A.; McGehee, M. D. Characterization of the Polymer Energy Landscape in Polymer:Fullerene Bulk Heterojunctions with Pure and Mixed Phases. *J. Am. Chem. Soc.* **2014**, *136*, 14078−14088.
(15) Bernardo, B.; Cheyns, D.; Verreet, B.; Schaller, R. D.; Rand, B. P.; Giebink, N. C. Delocalization and Dielectric Screening of Charge Transfer States in Organic Photovoltaic Cells. *Nat. Commun.* **2014**, *5*, 3245.
(16) Heitzer, H. M.; Savoie, B. M.; Marks, T. J.; Ratner, M. A. Organic Photovoltaics: Elucidating the Ultra-Fast Exciton Dissociation Mechanism in Disordered Materials. *Angew. Chem., Int. Ed.* **2014**, *53*, 7456−7460.
(17) *Physics of Organic Semiconductors*; Brütting, W., Adachi, C., Eds.; John Wiley & Sons: Weinheim, Germany, 2012.
(18) *Organic Photovoltaics: Materials, Device Physics, and Manufacturing Technologies*; Brabec, C.; Scherf, U.; Dyakonov, V., Eds.; John Wiley & Sons: Weinheim, Germany, 2014.
(19) Kaur, N.; Singh, M.; Pathak, D.; Wagner, T.; Nunzi, J. M. Organic Materials for Photovoltaic Applications: Review and Mechanism. *Synth. Met.* **2014**, *190*, 20−26.
(20) Bundgaard, E.; Krebs, F. C. Low Band Gap Polymers for Organic Photovoltaics. *Sol. Energy Mater. Sol. Cells* **2007**, *91*, 954−985.
(21) Kim, H.; Shin, M.; Kim, Y. Distinct Annealing Temperature in Polymer:Fullerene:Polymer Ternary Blend Solar Cells. *J. Phys. Chem. C* **2009**, *113*, 1620−1623.
(22) Koppe, M.; Egelhaaf, H.-J.; Dennler, G.; Scharber, M. C.; Brabec, C. J.; Schilinsky, P.; Hoth, C. N. Near IR Sensitization of Organic Bulk Heterojunction Solar Cells: Towards Optimization of the Spectral Response of Organic Solar Cells. *Adv. Funct. Mater.* **2010**, *20*, 338−346.
(23) Khlyabich, P. P.; Burkhart, B.; Thompson, B. C. Efficient Ternary Blend Bulk Heterojunction Solar Cells with Tunable Open-Circuit Voltage. *J. Am. Chem. Soc.* **2011**, *133*, 14534−14537.
(24) Wang, D. H.; Kim, D. Y.; Choi, K. W.; Seo, J. H.; Im, S. H.; Park, J. H.; Park, O. O.; Heeger, A. J. Enhancement of Donor-Acceptor Polymer Bulk Heterojunction Solar Cell Power Conversion Efficiencies by Addition of Au Nanoparticles. *Angew. Chem., Int. Ed.* **2011**, *50*, 5519−5523.
(25) Yang, L.; Zhou, H.; Price, S. C.; You, W. Parallel-Like Bulk Heterojunction Polymer Solar Cells. *J. Am. Chem. Soc.* **2012**, *134*, 5432−5435.
(26) Khlyabich, P. P.; Burkhart, B.; Thompson, B. C. Compositional Dependence of the Open-Circuit Voltage in Ternary Blend Bulk Heterojunction Solar Cells Based on Two Donor Polymers. *J. Am. Chem. Soc.* **2012**, *134*, 9074−9077.
(27) Li, Y. Molecular Design of Photovoltaic Materials for Polymer Solar Cells: Toward Suitable Electronic Energy Levels and Broad Absorption. *Acc. Chem. Res.* **2012**, *45*, 723−733.
(28) Ameri, T.; Khoram, P.; Min, J.; Brabec, C. J. Organic Ternary Solar Cells: A Review. *Adv. Mater. (Weinheim, Ger.)* **2013**, *25*, 4245−4266.
(29) Chen, Y.-C.; Hsu, C.-Y.; Lin, R. Y.-Y.; Ho, K.-C.; Lin, J. T. Materials for the Active Layer of Organic Photovoltaics: Ternary Solar Cell Approach. *ChemSusChem* **2013**, *6*, 20−35.
(30) Jung, J. W.; Liu, F.; Russell, T. P.; Jo, W. H. Semi-Crystalline Random Conjugated Copolymers with Panchromatic Absorption for Highly Efficient Polymer Solar Cells. *Energy Environ. Sci.* **2013**, *6*, 3301−3307.
(31) Griffith, O. L.; Forrest, S. R. Exciton Management in Organic Photovoltaic Multidonor Energy Cascades. *Nano Lett.* **2014**, *14*, 2353−2358.
(32) Ye, L.; Xu, H.-H.; Yu, H.; Xu, W.-Y.; Li, H.; Wang, H.; Zhao, N.; Xu, J.-B. Ternary Bulk Heterojunction Photovoltaic Cells Composed of Small Molecule Donor Additive as Cascade Material. *J. Phys. Chem. C* **2014**, *118*, 20094−20099.
(33) Placencia, D.; Wang, W.; Gantz, J.; Jenkins, J. L.; Armstrong, N. R. Highly Photoactive Titanyl Phthalocyanine Polymorphs as Textured Donor Layers in Organic Solar Cells. *J. Phys. Chem. C* **2011**, *115*, 18873−18884.
(34) Ferguson, A. J.; Kopidakis, N.; Shaheen, S. E.; Rumbles, G. Quenching of Excitons by Holes in Poly(3-Hexylthiophene) Films. *J. Phys. Chem. C* **2008**, *112*, 9865−9871.
(35) Saeki, A.; Koizumi, Y.; Aida, T.; Seki, S. Comprehensive Approach to Intrinsic Charge Carrier Mobility in Conjugated Organic Molecules, Macromolecules, and Supramolecular Architectures. *Acc. Chem. Res.* **2012**, *45*, 1193−1202.
(36) Savenije, T. J.; Ferguson, A. J.; Kopidakis, N.; Rumbles, G. Revealing the Dynamics of Charge Carriers in Polymer:Fullerene Blends Using Photoinduced Time-Resolved Microwave Conductivity. *J. Phys. Chem. C* **2013**, *117*, 24085−24103.
(37) Polli, D.; Lüer, L.; Cerullo, G. High-Time-Resolution Pump-Probe System with Broadband Detection for the Study of Time-Domain Vibrational Dynamics. *Rev. Sci. Instrum.* **2007**, *78*, 103108.
(38) Cowan, S. R.; Banerji, N.; Leong, W. L.; Heeger, A. J. Charge Formation, Recombination, and Sweep-Out Dynamics in Organic Solar Cells. *Adv. Funct. Mater.* **2012**, *22*, 1116−1128.
(39) Proctor, C. M.; Kuik, M.; Nguyen, T.-Q. Charge Carrier Recombination in Organic Solar Cells. *Prog. Polym. Sci.* **2013**, *38*, 1941−1960.
(40) Banerji, N. Sub-Picosecond Delocalization in the Excited State of Conjugated Homopolymers and Donor−Acceptor Copolymers. *J. Mater. Chem. C* **2013**, *1*, 3052−3066.
(41) Savenije, T. J.; Murthy, D. H. K.; Gunz, M.; Gorenflot, J.; Siebbeles, L. D. A.; Dyakonov, V.; Deibel, C. Absence of Postnanosecond Charge Carrier Relaxation in Poly(3-Hexylthiophene)/Fullerene Blends. *J. Phys. Chem. Lett.* **2011**, *2*, 1368−1371.
(42) de Haas, M. P.; Warman, J. M. Photon-Induced Molecular Charge Separation Studied by Nanosecond Time-Resolved Microwave Conductivity. *Chem. Phys.* **1982**, *73*, 35−53.
(43) Reid, O. G.; Nekuda Malik, J. A.; Latini, G.; Dayal, S.; Kopidakis, N.; Silva, C.; Stingelin, N.; Rumbles, G. The Influence of Solid-State Microstructure on the Origin and Yield of Long-Lived Photogenerated Charge in Neat Semiconducting Polymers. *J. Polym. Sci., Part B: Polym. Phys.* **2012**, *50*, 27−37.
(44) Mizuguchi, J.; Rihs, G.; Karfunkel, H. R. Solid-State Spectra of Titanylphthalocyanine as Viewed From Molecular Distortion. *J. Phys. Chem.* **1995**, *99*, 16217−16227.
(45) Gulbinas, V. Transient Absorption of Photoexcited Titanylphthalocyanine in Various Molecular Arrangements. *Chem. Phys.* **2000**, *261*, 469−479.
(46) Yonehara, H.; Etori, H.; Engel, M. K.; Tsushima, M.; Ikeda, N.; Ohno, T.; Pac, C. Fabrication of Various Ordered Films of Oxotitanium(IV) Phthalocyanine by Vacuum Deposition and Their Spectroscopic Behavior. *Chem. Mater.* **2001**, *13*, 1015−1022.
(47) Coppedè, N.; Toccoli, T.; Pallaoro, A.; Siviero, F.; Walzer, K.; Castriota, M.; Cazzanelli, E.; Iannotta, S. Polymorphism and Phase Control in Titanyl Phthalocyanine Thin Films Grown by Supersonic Molecular Beam Deposition. *J. Phys. Chem. A* **2007**, *111*, 12550−12558.
(48) Kratschmer, W.; Lamb, L. D.; Fostiropoulos, K.; Huffman, D. R. Solid C_{60}: A New Form of Carbon. *Nature* **1990**, *347*, 354−358.
(49) Capozzi, V.; Casamassima, G.; Lorusso, G. F.; Minafra, A.; Piccolo, R.; Trovato, T.; Valentini, A. Optical Spectra and Photoluminescence of C_{60} Thin Films. *Solid State Commun.* **1996**, *98*, 853−858.
(50) Zhang, H.; Wu, C.; Liang, L.; Chen, Y.; He, Y.; Zhu, Y.; Ke, N.; Xu, J. B.; Wong, S. P.; Wei, A.; et al. Structural, Morphological and Optical Properties of C_{60} Cluster Thin Films Produced by Thermal Evaporation Under Argon Gas. *J. Phys.: Condens. Matter* **2001**, *13*, 2883−2889.

DOI: 10.1021/acs.jpcb.5b00110
J. Phys. Chem. B 2015, 119, 7729−7739

(51) Brown, P. J.; Thomas, D. S.; Köhler, A.; Wilson, J. S.; Kim, J.-S.; Ramsdale, C. M.; Sirringhaus, H.; Friend, R. H. Effect of Interchain Interactions on the Absorption and Emission of Poly(3-Hexylthiophene). *Phys. Rev. B: Condens. Matter Mater. Phys.* **2003**, *67*, 064203.
(52) Scharsich, C.; Lohwasser, R. H.; Sommer, M.; Asawapirom, U.; Scherf, U.; Thelakkat, M.; Neher, D.; Köhler, A. Control of Aggregate Formation in Poly(3-Hexylthiophene) by Solvent, Molecular Weight, and Synthetic Method. *J. Polym. Sci., Part B: Polym. Phys.* **2012**, *50*, 442−453.
(53) Dicker, G.; de Haas, M. P.; Warman, J. M.; de Leeuw, D. M.; Siebbeles, L. D. A. The Disperse Charge-Carrier Kinetics in Regioregular Poly(3-Hexylthiophene). *J. Phys. Chem. B* **2004**, *108*, 17818−17824.
(54) Dicker, G. Photogeneration and Dynamics of Charge Carriers in the Conjugated Polymer Poly (3-Hexylthiophene). Ph.D. Dissertation, Delft University of Technology, Delft, Netherlands, 2004.
(55) O'Connor, B. T.; Reid, O. G.; Zhang, X.; Kline, R. J.; Richter, L. J.; Gundlach, D. J.; DeLongchamp, D. M.; Toney, M. F.; Kopidakis, N.; Rumbles, G. Morphological Origin of Charge Transport Anisotropy in Aligned Polythiophene Thin Films. *Adv. Funct. Mater.* **2014**, *24*, 3422−3431.
(56) Hoofman, R. J. O. M.; van der Laan, G. P.; de Haas, M. P.; Tanigaki, K. Charge Migration in Pulse-Irradiated Undoped C_{60} Powder Studied with the Time-Resolved Microwave Conductivity Technique. *Synth. Met.* **1997**, *86*, 2355−2356.
(57) de Haas, M. P.; Warman, J. M.; Anthopoulos, T. D.; de Leeuw, D. M. The Mobility and Decay Kinetics of Charge Carriers in Pulse-Ionized Microcrystalline PCBM Powder. *Adv. Funct. Mater.* **2006**, *16*, 2274−2280.
(58) Callahan, R. A.; Coffey, D. C.; Chen, D.; Clark, N. A.; Rumbles, G.; Walba, D. M. Charge Generation Measured for Fullerene−Helical Nanofilament Liquid Crystal Heterojunctions. *ACS Appl. Mater. Interfaces* **2014**, *6*, 4823−4830.
(59) Tsushima, M.; Ikeda, N.; Yonehara, H.; Etori, H.; Pac, C.; Ohno, T. A Charge-Separated Pair in Thin Crystals of Oxotitanium (IV) Phthalocyanine Revealed by Means of Femtosecond Time-Resolved Absorption. *Coord. Chem. Rev.* **2002**, *229*, 3−8.
(60) Tsushima, M.; Motojima, Y.; Ikeda, N.; Yonehara, H.; Etori, H.; Pac, C.; Ohno, T. Excitons and a Charge-Separated Pair in Thin Crystals of Oxotitanium(IV) Phthalocyanine as Revealed by Femtosecond Time-Resolved Absorption and Time-Correlated Single Photon Counting. *J. Phys. Chem. A* **2002**, *106*, 2256−2264.
(61) Lawson, D. R.; Feldheim, D. L.; Foss, C. A.; Dorhout, P. K.; Elliott, C. M.; Martin, C. R.; Parkinson, B. Near-IR Absorption Spectra for the Buckminsterfullerene Anions: An Experimental and Theoretical Study. *J. Electrochem. Soc.* **1992**, *139*, L68−L71.
(62) Kaneto, K.; Abe, T.; Takashima, W. Evolution of Absorption Spectra of C_{60} Film in Solid Electrolyte Cell During Electrochemical Reduction. *Solid State Commun.* **1995**, *96*, 259−264.
(63) Fukuzumi, S.; Suenobu, T.; Patz, M.; Hirasaka, T.; Itoh, S.; Fujitsuka, M.; Ito, O. Selective One-Electron and Two-Electron Reduction of C_{60} with NADH and NAD Dimer Analogues via Photoinduced Electron Transfer. *J. Am. Chem. Soc.* **1998**, *120*, 8060−8068.
(64) Ohno, T.; Kato, S.; Yamada, A.; Tanno, T. Electron Transfer Reactions of the Photoexcited Triplet State of Chloroaluminum Phthalocyanine with Aromatic Amines, Benzoquinones, and Coordination Compounds of Iron(II) and Iron(III). *J. Phys. Chem.* **1983**, *87*, 775−781.
(65) Ohno, T.; Kato, S. Electron-Transfer Reactions of Excited Phthalocyanines: Spin Restriction on Reaction Rate of Electron Transfer and Energy Transfer to Cobalt Compounds. *J. Phys. Chem.* **1984**, *88*, 1670−1674.
(66) Piris, J.; Dykstra, T. E.; Bakulin, A. A.; van Loosdrecht, P. H. M.; Knulst, W.; Trinh, M. T.; Schins, J. M.; Siebbeles, L. D. A. Photogeneration and Ultrafast Dynamics of Excitons and Charges in P3HT/PCBM Blends. *J. Phys. Chem. C* **2009**, *113*, 14500−14506.
(67) Guo, J.; Ohkita, H.; Benten, H.; Ito, S. Near-IR Femtosecond Transient Absorption Spectroscopy of Ultrafast Polaron and Triplet Exciton Formation in Polythiophene Films with Different Regioregularities. *J. Am. Chem. Soc.* **2009**, *131*, 16869−16880.
(68) Guo, J.; Ohkita, H.; Benten, H.; Ito, S. Charge Generation and Recombination Dynamics in Poly(3-Hexylthiophene)/Fullerene Blend Films with Different Regioregularities and Morphologies. *J. Am. Chem. Soc.* **2010**, *132*, 6154−6164.
(69) Yamamoto, S.; Yasuda, H.; Ohkita, H.; Benten, H.; Ito, S.; Miyanishi, S.; Tajima, K.; Hashimoto, K. Charge Generation and Recombination in Fullerene-Attached Poly(3-Hexylthiophene)-Based Diblock Copolymer Films. *J. Phys. Chem. C* **2014**, *118*, 10584−10589.
(70) Gorenflot, J.; Heiber, M. C.; Baumann, A.; Lorrmann, J.; Gunz, M.; Kämpgen, A.; Dyakonov, V.; Deibel, C. Nongeminate Recombination in Neat P3HT and P3HT:PCBM Blend Films. *J. Appl. Phys.* **2014**, *115*, 144502.
(71) Spano, F. C. Modeling Disorder in Polymer Aggregates: the Optical Spectroscopy of Regioregular Poly(3-Hexylthiophene) Thin Films. *J. Chem. Phys.* **2005**, *122*, 234701.
(72) Clark, J.; Silva, C.; Friend, R. H.; Spano, F. C. Role of Intermolecular Coupling in the Photophysics of Disordered Organic Semiconductors: Aggregate Emission in Regioregular Polythiophene. *Phys. Rev. Lett.* **2007**, *98*, 206406.
(73) Noriega, R.; Rivnay, J.; Vandewal, K.; Koch, F. P. V.; Stingelin, N.; Smith, P.; Toney, M. F.; Salleo, A. A General Relationship Between Disorder, Aggregation and Charge Transport in Conjugated Polymers. *Nat. Mater.* **2013**, *12*, 1038−1044.
(74) Shoaee, S.; Subramaniyan, S.; Xin, H.; Keiderling, C.; Tuladhar, P. S.; Jamieson, F.; Jenekhe, S. A.; Durrant, J. R. Charge Photogeneration for a Series of Thiazolo-Thiazole Donor Polymers Blended with the Fullerene Electron Acceptors PCBM and ICBA. *Adv. Funct. Mater.* **2013**, *23*, 3286−3298.
(75) Ohkita, H.; Cook, S.; Astuti, Y.; Duffy, W.; Tierney, S.; Zhang, W.; Heeney, M.; McCulloch, I.; Nelson, J.; Bradley, D. D. C.; et al. Charge Carrier Formation in Polythiophene/Fullerene Blend Films Studied by Transient Absorption Spectroscopy. *J. Am. Chem. Soc.* **2008**, *130*, 3030−3042.
(76) Law, W.-F.; Lui, K. M.; Ng, D. K. P. Preparation, Solution Behaviour and Electrical Properties of Octasubstituted Phthalocyaninato and 2,3-Naphthalocyaninato Oxotitanium(IV) Complexes. *J. Mater. Chem.* **1997**, *7*, 2063−2067.
(77) Osterbacka, R.; An, C. P.; Jiang, X. M.; Vardeny, Z. V. Two-Dimensional Electronic Excitations in Self-Assembled Conjugated Polymer Nanocrystals. *Science* **2000**, *287*, 839−842.
(78) Korovyanko, O. J.; Osterbacka, R.; Jiang, X. M.; Vardeny, Z. V.; Janssen, R. A. J. Photoexcitation Dynamics in Regioregular and Regiorandom Polythiophene Films. *Phys. Rev. B: Condens. Matter Mater. Phys.* **2001**, *64*, 235122.

DOI: 10.1021/acs.jpcb.5b00110
J. Phys. Chem. B 2015, 119, 7729−7739